

The QSE-reduced α Network

W. Raphael Hix

Department of Astronomy, University of Texas, Austin, TX 78712

and

Alexei M. Khokhlov

Laboratory for Computational Physics and Fluid Dynamics, Code 6404, Naval Research
Laboratory, Washington, DC 20735

and

J. Craig Wheeler

Department of Astronomy, University of Texas, Austin, TX 78712

and

Friedrich-Karl Thielemann

Department of Physics & Astronomy, University of Basel, Klingelberstrasse 82, CH-4056
Basel Switzerland

ABSTRACT

Examination of the process of silicon burning, the burning stage that leads to the production of the iron peak nuclei, reveals that the nuclear evolution is dominated by large groups of nuclei in mutual equilibrium. These quasi-equilibrium (QSE) groups form well in advance of the global Nuclear Statistical Equilibrium (NSE). We present an improved “minimal” nuclear network, which takes advantage of quasi-equilibrium in order to calculate the nuclear evolution and energy generation while further reducing the computational cost compared to a conventional α -chain network. During silicon burning, the resultant *QSE-reduced* α network is twice as fast as the full α network it replaces and requires the tracking of only half as many abundance variables, without significant loss of accuracy. When the QSE-reduced α network is used in combination with a conventional α network stretching from He to Si, the combined $\alpha 7$ network provides an accurate approximation for all of the burning stages from He burning to NSE, while tracking only 7 abundances. These reductions in computational cost and the number of species evolved make the $\alpha 7$ network well suited for inclusion within hydrodynamic simulations, particularly those in multi-dimension.

Subject headings: methods: numerical — nuclear reactions, nucleosynthesis, abundances — stars: evolution — supernovae: general

1. Introduction

Nucleosynthesis calculations perform two functions in astrophysical models. The most important function, in the context of the evolution of the encompassing hydrodynamic model, is the calculation of the rate of thermonuclear energy generation. Where nucleosynthesis occurs, it is often the dominant source of energy, making careful determination of this rate of energy generation vital to accurate hydrodynamic modeling. The second function of a nucleosynthesis calculation is to determine the evolution of the nuclear species. For nuclear astrophysics and our understanding of the origin of the elements, this is of paramount importance. Often the best comparisons of model calculations with observations also depend on detailed knowledge of the abundances of nuclear species. Unfortunately, accurate calculation of the nuclear evolution is computationally expensive. For this reason, it is common to include within a hydrodynamic model only a limited approximation for nuclear burning which estimates the rate of energy generation. The detailed nuclear evolution is then calculated at a later time using the thermodynamic trajectories from the hydrodynamic model. Such a scheme is referred to as post-processing nucleosynthesis. The success of such a post-processing scheme depends largely on the accuracy with which the limited approximation which is included within the dynamical calculation can estimate the rate of energy generation. Frequently this inline nuclear burning calculation is a small network, trading a limited ability to follow the nuclear evolution for speed.

Tracking the nuclear evolution from helium burning through to NSE requires a network that includes nuclei from α -particles to Zn. Silicon burning presents a particular problem as material proceeds from silicon to the iron peak not via heavy ion captures but through a chain of photodisintegrations and light particle captures. The minimal nuclear set which can follow this evolution is the set of α -particle nuclei; α , ^{12}C , ^{16}O , ^{20}Ne , ^{24}Mg , ^{28}Si , ^{32}S , ^{36}Ar , ^{40}Ca , ^{44}Ti , ^{48}Cr , ^{52}Fe , ^{56}Ni , ^{60}Zn . For convenience we will label this full set \mathcal{F} and refer to its abundance as $\vec{Y}^{\mathcal{F}}$. Silicon burning in fact presents a larger problem, as the nuclear flow from silicon to the iron peak nuclei does not generally proceed through nuclei with $N=Z$, especially when significant neutronization has occurred (Hix & Thielemann 1996 : henceforth HT96). In some models, however, such compromise is made necessary by the computational limitations.

The nature of nuclear network calculations has been extensively reviewed elsewhere (see, e.g., Woosley 1986, Thielemann et al. 1994 or Arnett 1996), so we will discuss it only briefly here. From a set of nuclear abundances, and the reaction rates for the reactions which link them, one can calculate the time derivatives of the abundances, \dot{Y} . With these derivatives, the abundances of the included nuclei, at time t , and over timestep Δt , are evolved according to the finite difference prescription

$$\frac{\vec{Y}(t + \Delta t) - \vec{Y}(t)}{\Delta t} = \begin{array}{l} \dot{\vec{Y}}(t) \quad (\textit{explicit}) \\ \dot{\vec{Y}}(t + \Delta t) \quad (\textit{implicit}) . \end{array} \quad (1)$$

For the stiff set of non-linear differential equations which form most nuclear networks, a fully implicit treatment is most successful. Solving the implicit version of Eq. 1 is equivalent to finding the zeros of the set of equations

$$\vec{Z}(t + \Delta t) \equiv \frac{\vec{Y}(t + \Delta t) - \vec{Y}(t)}{\Delta t} - \dot{\vec{Y}}(t + \Delta t) = 0 . \quad (2)$$

This is done using the Newton-Raphson method (see, e.g., Press, et al., 1992), which is based on the Taylor series expansion of $\vec{Z}(t + \Delta t)$, with the trial change in abundances given by

$$\Delta \vec{Y} = \left(\frac{\partial \vec{Z}(t + \Delta t)}{\partial \vec{Y}(t + \Delta t)} \right)^{-1} \vec{Z} , \quad (3)$$

where $\partial \vec{Z} / \partial \vec{Y}$ is the Jacobian of \vec{Z} . Iteration continues until $\vec{Y}(t + \Delta t)$ converges.

The conclusion of silicon burning with nuclear statistical equilibrium (NSE) offers a hint to a more efficient means of evolving nuclear abundances, since the equilibrium distribution reduces the number of independent variables which must be tracked. NSE grows from several groups of nuclei which form local equilibria. The existence of these quasi-equilibrium groups frees one from accounting for the changes in the abundances of each of the members of these groups, as the changes within the groups can be accounted for by the changes of a few crucial abundances. Previous authors, most notably Bodansky, Clayton & Fowler (1968: henceforth BCF), have attempted to use quasi-equilibrium to simplify the calculation of silicon burning. Having noted the computational difficulties encountered by Turan et al. (1966) in their pioneering nuclear network study of silicon burning, BCF sought to model silicon burning with a single quasi-equilibrium group, stretching from ^{24}Mg and ^{28}Si through the iron peak nuclei. BCF postulated that the downward flow from this group occurred via $^{24}\text{Mg}(\gamma, \alpha)^{20}\text{Ne}$ and that the flow of α -particles downward through ^{20}Ne , ^{16}O , and ^{12}C conserved the abundances of these nuclei. From these assumptions, they derived expressions for the abundances of these light α -particle

nuclei and for the downward flux of α -particles which depended only on the abundances of α -particles and ^{28}Si . Though this model was moderately successful in replicating the abundance pattern found in the solar system from $A=30$ to $A=60$, it had clear limitations when compared to the network calculations of TCG, particularly at early times when the assumption of conservative flow was most suspect. Woosley, Arnett, & Clayton (1973: henceforth WAC) concluded that such efforts were at best marginally successful, in part because as matter cools the photodisintegration reactions freeze out well before the particle captures cease, thereby destroying quasi-equilibrium. WAC found a further complication in that, at early times, their models exhibited two separate QSE groups, one around silicon and the other containing the iron peak nuclei. WAC did demonstrate that, with the assumption of QSE, reasonable estimates of the time required to merge the two QSE groups and the time to reach silicon exhaustion could be calculated. HT96 demonstrated additional complications as both the path of the nuclear flow from the silicon group to the iron peak group and the membership of these groups depended strongly on the amount of neutronization. HT96 further demonstrated that for material which has undergone significant neutronization, the separation between the silicon and iron peak groups persists through a significant part of the nuclear evolution. In spite of these complications, Hix & Thielemann (1998: henceforth HT98) showed that QSE could provide a reasonable estimate of the abundances of many species during silicon burning, even under explosive conditions, where the photodisintegration reactions freeze out before their corresponding particle captures. Arnett 1996 provides a more complete history of the use of QSE.

2. The QSE-reduced Network

The objective of the QSE-reduced α network is to evolve $\vec{Y}^{\mathcal{F}}$ during silicon burning, and calculate the resulting energy generation, in a more efficient way. Under conditions where QSE applies, the existence of the silicon and iron peak QSE groups allows calculation of the abundances of these 14 nuclei from a reduced set of 7 abundances. For the members of the silicon group (^{28}Si , ^{32}S , ^{36}Ar , ^{40}Ca , ^{44}Ti), the individual abundances can be calculated from the assumption of QSE by

$$Y_{QSE,\text{Si}}(^AZ) = \frac{C(^AZ)}{C(^{28}\text{Si})} Y(^{28}\text{Si}) Y_\alpha^{\frac{A-28}{4}}, \quad (4)$$

where we have defined

$$C(^AZ) = \frac{G(^AZ)}{2^A} \left(\frac{\rho N_A}{\theta} \right)^{A-1} A^{\frac{3}{2}} \exp\left(\frac{B(^AZ)}{k_B T} \right), \quad (5)$$

for later convenience and

$$\theta = \left(\frac{m_u k_B T}{2\pi\hbar^2} \right)^{3/2} .$$

The functions $G(^A Z)$ and $B(^A Z)$ are the partition function and binding energy of the nucleus $^A Z$, N_A is Avagadro’s number, k_B is Boltzmann’s constant, and ρ and T are the density and temperature of the plasma. Y_α is the abundance of free α -particles and the integer $(A - 28)/4$ is the number of α -particles needed to construct $^A Z$ from ^{28}Si . Similarly, the abundances of the members of the iron peak group (^{48}Cr , ^{52}Fe , ^{56}Ni , ^{60}Zn) can be calculated by

$$Y_{QSE, \text{Ni}}(^A Z) = \frac{C(^A Z)}{C(^{56}\text{Ni})} Y(^{56}\text{Ni}) Y_\alpha^{\frac{A-56}{4}} . \quad (6)$$

Thus, under conditions where QSE applies, $\vec{Y}^{\mathcal{F}}$ can be expressed as a function of the abundances of the reduced nuclear set \mathcal{R} , defined as $[\alpha, ^{12}\text{C}, ^{16}\text{O}, ^{20}\text{Ne}, ^{24}\text{Mg}, ^{28}\text{Si}, ^{56}\text{Ni}]$, and it is therefore sufficient to evolve only $\vec{Y}^{\mathcal{R}}$. It should be noted that WAC and HT96 have shown that ^{24}Mg is ordinarily a member of the silicon QSE group during silicon burning, leaving only 6 independant abundances, but for ease in integration with the conventional nuclear network which we will discuss in §4, we will evolve the ^{24}Mg abundance independantly (see Arnett 1996).

While $\vec{Y}^{\mathcal{R}}$ is a convenient set of abundances for the calculation of $\vec{Y}^{\mathcal{F}}$, it is not the most efficient set to evolve, primarily because of the complexity of calculating the necessary time derivatives and their Jacobian. It is much easier to calculate the time derivatives of each QSE group as a whole. To this end, we define $\vec{Y}^{\mathcal{G}} = [Y_{\alpha G}, Y(^{12}\text{C}), Y(^{16}\text{O}), Y(^{20}\text{Ne}), Y(^{24}\text{Mg}), Y_{SiG}, Y_{FeG}]$, where

$$\begin{aligned} Y_{\alpha G} &= Y_\alpha + \sum_{i \in \text{Si group}} \frac{A_i - 28}{4} Y_i + \sum_{i \in \text{Fe group}} \frac{A_i - 56}{4} Y_i , \\ Y_{SiG} &= \sum_{i \in \text{Si group}} Y_i , \\ Y_{FeG} &= \sum_{i \in \text{Fe group}} Y_i . \end{aligned} \quad (7)$$

Physically, Y_{SiG} and Y_{FeG} represent the total abundances of the silicon and iron peak QSE groups, while $Y_{\alpha G}$ represents the sum of the abundances of free α -particles and those α -particles required to build the members of the QSE groups from ^{28}Si or ^{56}Ni .

Employing the group abundance set \mathcal{G} also reduces the number of reactions whose flux must be calculated since quasi-equilibrium allows one to ignore the reactions among the members of the QSE groups. Unfortunately, the rates for this reduced set of reactions are

still functions of $\vec{Y}^{\mathcal{F}}$. For example, the nuclear flux into the iron peak group,

$$\dot{Y}_{FeG} = \rho\langle\sigma v\rangle Y_{\alpha} Y(^{44}\text{Ti}) - \lambda Y(^{48}\text{Cr}) , \quad (8)$$

depends not on the group abundances, $Y_{\alpha G}$, Y_{SiG} and Y_{FeG} , but on the abundances of free α -particles, ^{44}Ti , and ^{48}Cr . Since these time derivatives are not easily expressed in terms of $\vec{Y}^{\mathcal{G}}$, one must calculate $\dot{\vec{Y}}^{\mathcal{G}}$ from $\vec{Y}^{\mathcal{F}}$ or alternately, using Eqs. 4 and 6, from $\vec{Y}^{\mathcal{R}}$. Applying Eqs. 4 and 6 to Eq. 8 results in

$$\dot{Y}_{FeG} = \rho\langle\sigma v\rangle \frac{C(^{44}\text{Ti})}{C(^{28}\text{Si})} Y(^{28}\text{Si}) Y_{\alpha}^5 - \lambda \frac{C(^{48}\text{Cr})}{C(^{56}\text{Ni})} Y(^{56}\text{Ni}) Y_{\alpha}^{-2} . \quad (9)$$

Thus, to evolve $\vec{Y}^{\mathcal{G}}$ over time, one must repeatedly solve for $\vec{Y}^{\mathcal{R}}$. By applying Eqs. 4 and 6 to Eq. 7, one may write $\vec{Y}^{\mathcal{G}}$ as a function of $\vec{Y}^{\mathcal{R}}$, with seven independant equations for the seven abundances of $\vec{Y}^{\mathcal{R}}$ implying a unique relation between $\vec{Y}^{\mathcal{G}}$ and $\vec{Y}^{\mathcal{R}}$. Fortunately, with the exception of Y_{α} , the relations between $\vec{Y}^{\mathcal{G}}$ and $\vec{Y}^{\mathcal{R}}$ are linear.

Further complicating the calculation, however, is the need in Eq. 3 for the Jacobian of \vec{Z} . This requires knowledge of $\partial\dot{\vec{Y}}^{\mathcal{G}}/\partial\vec{Y}^{\mathcal{G}}$, which can not be calculated directly since $\dot{\vec{Y}}^{\mathcal{G}}$ can not be expressed in terms of $\vec{Y}^{\mathcal{G}}$. Instead, we have been successful using the chain rule,

$$\frac{\partial\dot{\vec{Y}}^{\mathcal{G}}}{\partial\vec{Y}^{\mathcal{G}}} = \frac{\partial\dot{\vec{Y}}^{\mathcal{G}}}{\partial\vec{Y}^{\mathcal{R}}} \frac{\partial\vec{Y}^{\mathcal{R}}}{\partial\vec{Y}^{\mathcal{G}}} \quad (10)$$

to calculate the Jacobian. Analytically, the first term on the righthand side of Eq. 10 is easily calculated from the sums of reaction terms. For example, from Eq. 9 we can see that the non-zero terms of $\partial\dot{Y}_{FeG}/\partial\vec{Y}^{\mathcal{R}}$ are

$$\begin{aligned} \frac{\partial\dot{Y}_{FeG}}{\partial Y_{\alpha}} &= 5\langle\sigma v\rangle \frac{C(^{44}\text{Ti})}{C(^{28}\text{Si})} Y(^{28}\text{Si}) Y_{\alpha}^4 + 2\lambda \frac{C(^{48}\text{Cr})}{C(^{56}\text{Ni})} Y(^{56}\text{Ni}) Y_{\alpha}^{-3} , \\ \frac{\partial\dot{Y}_{FeG}}{\partial Y(^{28}\text{Si})} &= \langle\sigma v\rangle \frac{C(^{44}\text{Ti})}{C(^{28}\text{Si})} Y_{\alpha}^5 \quad \text{and} \quad \frac{\partial\dot{Y}_{FeG}}{\partial Y(^{56}\text{Ni})} = \lambda \frac{C(^{48}\text{Cr})}{C(^{56}\text{Ni})} Y_{\alpha}^{-2} . \end{aligned} \quad (11)$$

Calculation of the second term on the righthand side of Eq. 10 is more complicated, requiring implicit differentiation of the definition of $\vec{Y}^{\mathcal{G}}$ with respect to $\vec{Y}^{\mathcal{G}}$, using Eq. 7. As an example, in order to calculate $\partial\dot{Y}_{FeG}/\partial Y_{FeG}$, we differentiate Eq. 7 with respect to Y_{FeG} , resulting in 3 equations for three unknowns, $\partial Y_{\alpha}/\partial Y_{FeG}$, $\partial Y(^{28}\text{Si})/\partial Y_{FeG}$, and $\partial Y(^{56}\text{Ni})/\partial Y_{FeG}$, while the other 4 terms of $\partial\dot{\vec{Y}}^{\mathcal{R}}/\partial Y_{FeG}$ are manifestly zero. Solving these 3 equations results in the 3 terms

$$\frac{\partial Y_{\alpha}}{\partial Y_{FeG}} = -\frac{\mathcal{M}_{Fe}^1}{\mathcal{M}_{Fe}^0} \mathcal{M}_{\alpha}^{-1}$$

$$\begin{aligned} \frac{\partial Y(^{28}\text{Si})}{\partial Y_{FeG}} &= \frac{Y(^{28}\text{Si})}{Y_\alpha} \frac{\mathcal{M}_{Si}^1}{\mathcal{M}_{Si}^0} \frac{\mathcal{M}_{Fe}^1}{\mathcal{M}_{Fe}^0} \mathcal{M}_\alpha^{-1} \\ \frac{\partial Y(^{56}\text{Ni})}{\partial Y_{FeG}} &= \frac{Y(^{56}\text{Ni})}{\mathcal{M}_{Fe}^0} \left(1 + \frac{\mathcal{M}_{Fe}^{1\ 2}}{\mathcal{M}_{Fe}^0} \frac{\mathcal{M}_\alpha^{-1}}{Y_\alpha} \right). \end{aligned} \quad (12)$$

where we have used the following definitions for simplification

$$\begin{aligned} \mathcal{M}_{Si}^j &= \sum_{i \in Si\ Group} \left(\frac{A-28}{4} \right)^j Y_i, & \mathcal{M}_{Fe}^j &= \sum_{i \in Fe\ Group} \left(\frac{A-56}{4} \right)^j Y_i \\ \mathcal{M}_\alpha &= 1 + \frac{1}{Y_\alpha} \left(\mathcal{M}_{Si}^2 + \mathcal{M}_{Fe}^2 - \frac{\mathcal{M}_{Si}^{1\ 2}}{\mathcal{M}_{Si}^0} - \frac{\mathcal{M}_{Fe}^{1\ 2}}{\mathcal{M}_{Fe}^0} \right). \end{aligned} \quad (13)$$

Multiplying each term in Eq. 12 by the respective component of Eq. 11 and summing produces $\partial \dot{Y}_{FeG} / \partial Y_{FeG}$.

3. Silicon burning with the QSE-reduced α network

In this section we will demonstrate the accuracy with which the QSE-reduced α network duplicates the results of the full 14 element α network for silicon burning. Our first examples are nucleosynthesis calculations occurring under constant temperature and density. While these calculations provide the least challenging comparison, they also allow comparison with NSE, which should represent the final abundances of these calculations. Figure 1 offers comparison of the mass fractions of the 7 independent species; α -particles, ^{12}C , ^{16}O , ^{20}Ne , ^{24}Mg , and the silicon and iron peak groups, as evolved by the QSE-reduced and conventional α networks for silicon burning at 5×10^9 K and a density of 10^9 g cm $^{-3}$. Apart from an early enhancement by the QSE-reduced network of the iron peak mass fraction (20% after 10^{-6} seconds), these mass fractions typically agree to within 1%. Since the nuclear energy release depends linearly on the abundance changes, differences in small abundances have little effect on the nuclear energy store. In this case, the difference in the rate of energy generation calculated by the two networks is $< 1\%$ at 10^{-6} and 10^{-4} seconds. This difference is significantly smaller than the variation, shown by both networks, in the rate of energy generation between timesteps, with $\dot{\epsilon}$ typically declining by 5% per timestep over this interval.

With such good agreement between the respective abundances of free α -particles and the two QSE group abundances, significant variations in abundance among the individual members of the QSE groups can only result from deviations from QSE. At early times, the small abundances within the iron peak reduce the accuracy of QSE at predicting the individual abundances of members of the iron peak group. Much of the enhanced mass

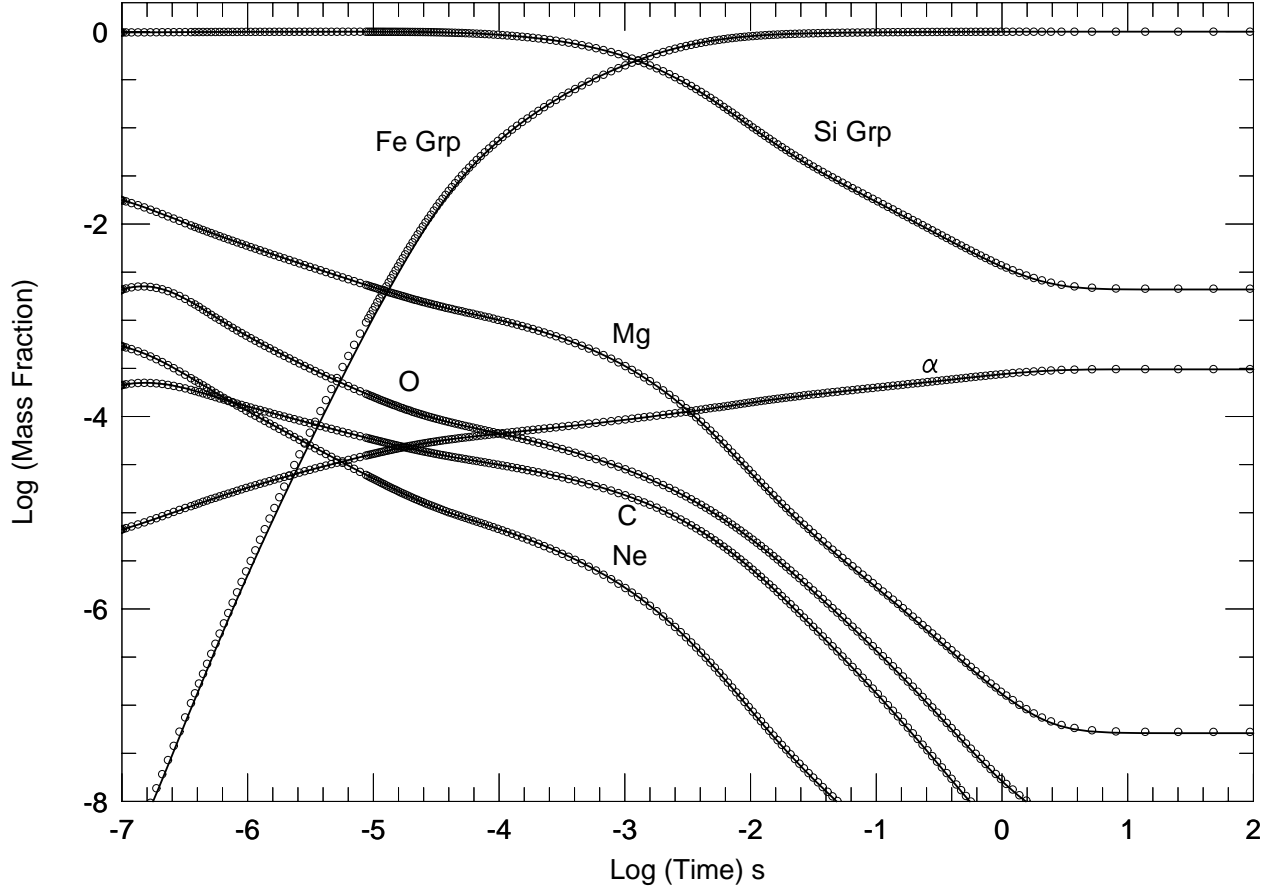


Fig. 1.— Evolution of the independent nuclear mass fractions for constant thermodynamic conditions, $T_9=5$ and $\rho = 10^9 \text{ g cm}^{-3}$. The solid lines display the evolution due to a conventional α network, the circles show the evolution by the QSE-reduced α network. The Silicon group mass fraction is the sum of the mass fractions of ^{28}Si , ^{32}S , ^{36}Ar , ^{40}Ca , and ^{44}Ti . The Iron group mass fraction is the sum of the mass fractions of ^{48}Cr , ^{52}Fe , ^{56}Ni , and ^{60}Zn .

fraction of the iron peak nuclei at early times, seen in Fig. 1, is due to the QSE-reduced network’s emphasis on heavier nuclei at the expense of ^{48}Cr . After an elapsed time of 10^{-6} seconds, the average mass of the iron peak nuclei, \bar{A}_{FeG} , is 49.2 according to the conventional network and 52.6 according to the QSE-reduced network. As a result, the abundances of ^{48}Cr and ^{52}Fe calculated by the QSE-reduced network are 38% and 164% of their conventional network values, while ^{56}Ni and ^{60}Zn are 16 times more abundant than the conventional network predicts. As the iron peak nuclei become more abundant, QSE provides a better estimate of the relative abundances within the group, reducing such discrepancies. By the time the iron peak nuclei represent a significant portion of the mass, the differences in the abundance predictions for all nuclei are only a few per cent. Comparison of columns 2 and 3 of Table 1 show that after an elapsed time of 10^{-4} seconds, ^{48}Cr displays the largest difference, with the QSE-reduced network’s abundance equal to 97% of the abundance calculated by the conventional network. In the context of the network evolution, this small difference is less than half of the abundance change for ^{48}Cr that occurs over the following timestep. As each network reaches its respective equilibria the abundance predictions of these networks continue to differ by at most 3%, even among the nuclei with the smallest abundances. Not surprisingly, in view of these small abundance differences, the difference in the total energy released by these networks is less than .1%. Comparison of the network abundances with abundances calculated from NSE show a similarly low level of difference. It should be noted that these NSE abundances, calculated assuming that the α nuclei are the only available states in the equilibrium, differ noticeably from NSE calculations which include all nuclei, even for $Y_e = 0.5$.

For higher temperatures, large abundances of free α -particles reduce the importance of the silicon and iron peak nuclei. As Column 4 of Table 2 reveals, even the NSE abundance distribution which represents the end point of silicon burning may be dominated by free α -particles. In spite of the larger role played by free α -particles, the QSE-reduced α network successfully replicates the nuclear evolution during silicon burning, because the nuclei of the silicon and iron peak groups still obey QSE. Fig. 2 compares the nuclear evolution of the independent mass fractions from the QSE-reduced α network to their conventional counterparts, with $T_9=6$ and $\rho = 10^7 \text{ g cm}^{-3}$. Here too, the iron group mass fraction is initially over-predicted by the QSE-reduced network, though to a lesser extent (7% after 10^{-8} seconds). This over-prediction also subsides as the iron peak abundances increase, and hence their adherence to QSE improves. As in the previous case, despite these small differences in abundance, the agreement between the rates of energy generation is better than 1%. Examination of Table 2 reveals that the equilibrium abundances for the individual nuclei calculated by the QSE-reduced network also agree well with those calculated by the conventional network and by NSE. Even for the smallest abundances, the differences are

Table 1: Comparison between the QSE-reduced and conventional network abundances after 1.06×10^{-4} seconds with $T_9=5$ and $\rho = 10^9 \text{ g cm}^{-3}$

Nucleus	Y_{net}	Y_{qse}
^4He	1.67×10^{-5}	1.68×10^{-5}
^{12}C	2.59×10^{-6}	2.58×10^{-6}
^{16}O	4.09×10^{-6}	4.09×10^{-6}
^{20}Ne	3.29×10^{-7}	3.28×10^{-7}
^{24}Mg	4.11×10^{-5}	4.11×10^{-9}
^{28}Si	1.88×10^{-2}	1.89×10^{-2}
^{32}S	8.40×10^{-3}	8.36×10^{-3}
^{36}Ar	2.07×10^{-3}	2.04×10^{-3}
^{40}Ca	1.27×10^{-3}	1.24×10^{-3}
^{44}Ti	1.52×10^{-5}	1.48×10^{-6}
^{48}Cr	5.63×10^{-5}	5.45×10^{-5}
^{52}Fe	2.67×10^{-4}	2.69×10^{-4}
^{56}Ni	1.11×10^{-3}	1.13×10^{-3}
^{60}Zn	6.65×10^{-8}	6.73×10^{-8}

Table 2: Comparison of network abundances at freezeout with NSE for $T_9=6$ and $\rho = 10^7 \text{ g cm}^{-3}$

Nucleus	Y_{net}	Y_{qse}	Y_{nse}
^4He	1.23×10^{-1}	1.24×10^{-1}	1.25×10^{-1}
^{12}C	1.03×10^{-6}	1.04×10^{-6}	1.04×10^{-6}
^{16}O	1.88×10^{-6}	1.91×10^{-6}	1.89×10^{-6}
^{20}Ne	3.54×10^{-8}	3.62×10^{-8}	3.56×10^{-8}
^{24}Mg	4.08×10^{-6}	4.18×10^{-6}	4.08×10^{-6}
^{28}Si	1.28×10^{-3}	1.32×10^{-3}	1.28×10^{-3}
^{32}S	1.21×10^{-3}	1.23×10^{-3}	1.20×10^{-3}
^{36}Ar	7.03×10^{-4}	7.13×10^{-4}	7.00×10^{-4}
^{40}Ca	7.60×10^{-4}	7.64×10^{-4}	7.55×10^{-4}
^{44}Ti	4.16×10^{-5}	4.14×10^{-5}	4.12×10^{-5}
^{48}Cr	2.70×10^{-4}	2.71×10^{-4}	2.67×10^{-4}
^{52}Fe	1.43×10^{-3}	1.42×10^{-3}	1.41×10^{-3}
^{56}Ni	5.13×10^{-3}	5.06×10^{-3}	5.06×10^{-3}
^{60}Zn	2.98×10^{-6}	2.92×10^{-6}	2.94×10^{-6}

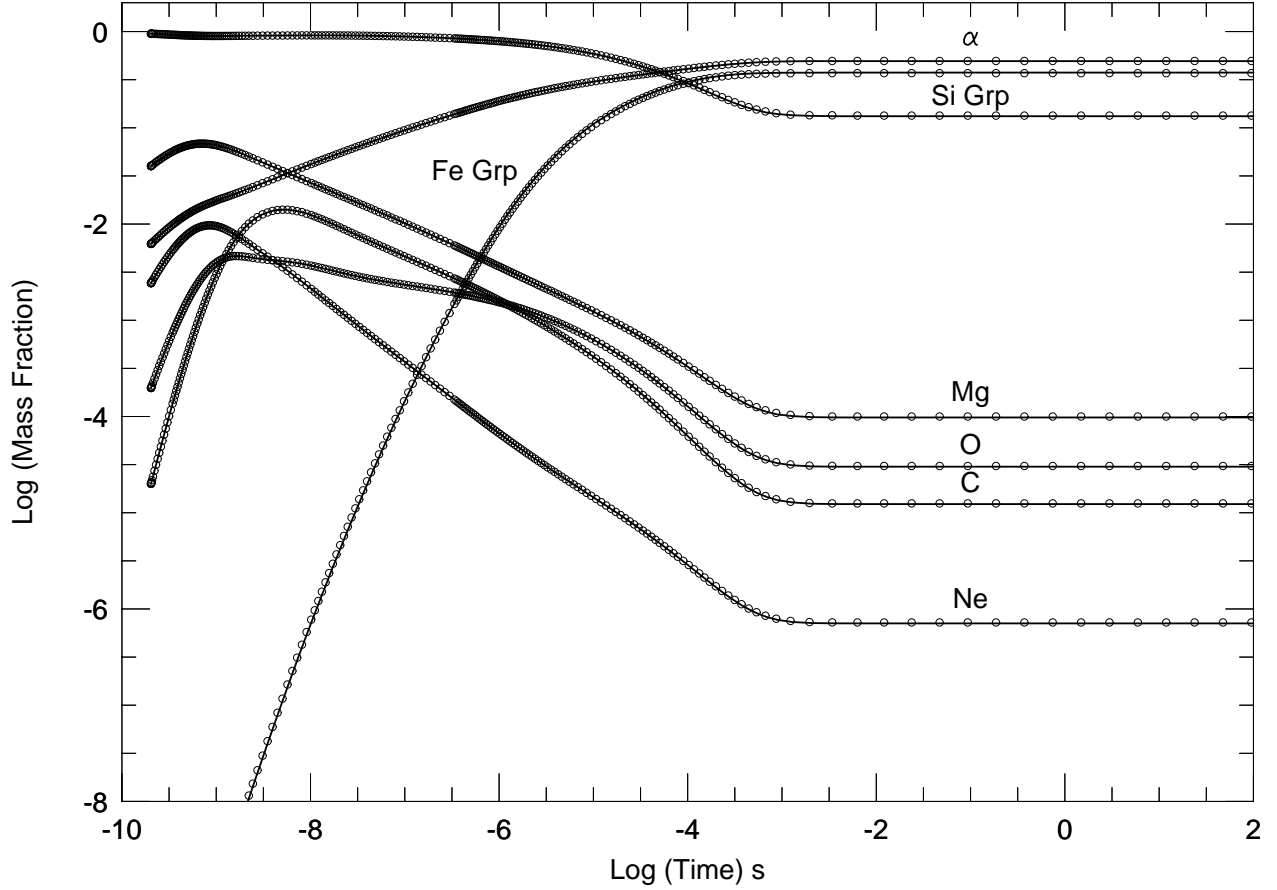


Fig. 2.— Evolution of the independent nuclear mass fractions for constant thermodynamic conditions, $T_9=6$ and $\rho = 10^7 \text{ g cm}^{-3}$. The solid lines display the evolution due to a conventional α network, the circles show the evolution by the QSE-reduced α network. The Silicon group mass fraction is the sum of the mass fractions of ^{28}Si , ^{32}S , ^{36}Ar , ^{40}Ca , and ^{44}Ti . The Iron group mass fraction is the sum of the mass fractions of ^{48}Cr , ^{52}Fe , ^{56}Ni , and ^{60}Zn .

less than 3%.

While examples of silicon burning calculations under constant conditions are instructive, if the QSE-reduced α network is to replace the conventional α network it must be shown to be accurate under changing thermodynamic conditions. Of particular importance is the ability to model explosive silicon burning. As a representative analytic model for silicon burning occurring as a result of shock heating, we will consider a mass zone which is instantaneously heated by a passing shock to some peak initial temperature T_{9i} and density ρ_i and then expands and cools adiabatically. Following the approximation introduced by Fowler & Hoyle (1964), the hydrodynamic expansion timescale (equal to the free fall timescale) is

$$\tau_{\text{HD}} = (24\pi G\rho)^{-1/2} = 446\rho_6^{-1/2}\text{ms}, \quad (14)$$

with the time dependence of the density and temperature of this radiation dominated gas given by

$$\begin{aligned} \rho(t) &= \rho_i \exp(-t/\tau_{\text{HD}}), \\ T_9(t) &= T_{9i} \exp(-t/3\tau_{\text{HD}}), \end{aligned} \quad (15)$$

assuming the adiabatic exponent $\gamma = 4/3$. For initial conditions we chose conditions identical to the examples discussed above.

Figure 3 shows the nuclear evolution for an example of this explosive burning model with $T_{9i} = 5$ and $\rho_i = 10^9 \text{ g cm}^{-3}$. Over the first millisecond, the evolution portrayed here is virtually identical to that of Figure 1; however by the time one millisecond has elapsed, the temperature has dropped to $4.9 \times 10^9 \text{ K}$, slowing the reactions which are turning silicon into iron peak elements. This cooling, which drops T_9 below 4 after 9 ms and below 3 after 22 ms, freezes out the nuclear reactions before NSE is reached, resulting in incomplete silicon burning, as discussed by WAC. In this case, the freezeout leaves nearly equal amounts of silicon group and iron peak group elements. Throughout most of the evolution in this example, the agreement between the mass fractions as evolved by the QSE-reduced α network with those evolved by its conventional counterpart is comparable to that demonstrated under constant thermodynamic conditions. Columns 2 and 3 of Table 3 compare the abundances after 9 ms have elapsed, with T_9 nearing 4. In this case, as for that displayed in Table 1, the largest relative error (5%) is in the abundance of ^{48}Cr . These small differences in abundance result in small differences in the accumulated nuclear energy release, approximately .5% to this point. By this time, adiabatic cooling has greatly reduced the rate of energy generation from its peak of more than $10^{22} \text{ ergs g}^{-1} \text{ s}^{-1}$ to roughly $10^{17} \text{ ergs g}^{-1} \text{ s}^{-1}$. Though the absolute difference in the rate of energy generation as calculated by the 2 networks has declined from $\sim 10^{19}$ to $10^{16} \text{ ergs g}^{-1} \text{ s}^{-1}$, the relative

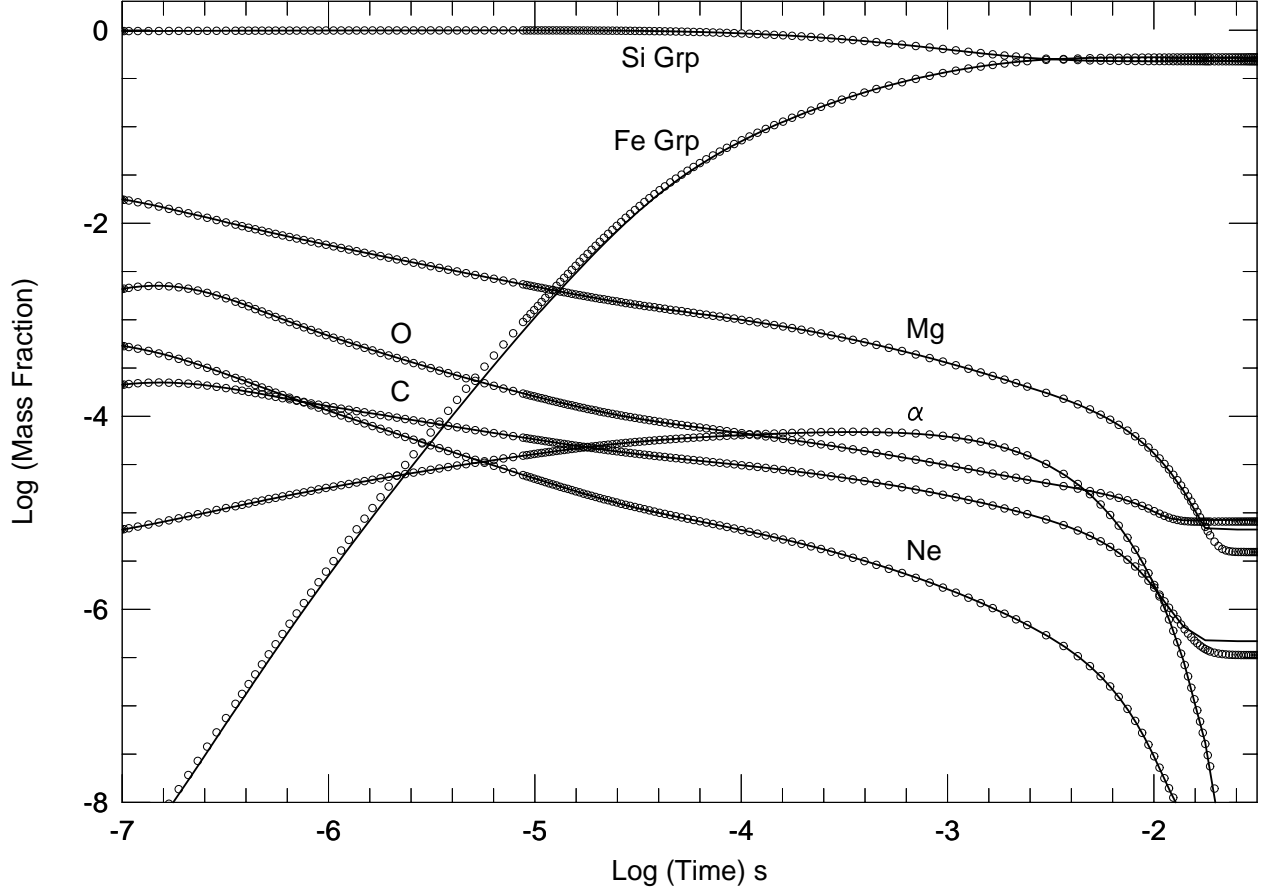


Fig. 3.— Evolution of the independent nuclear mass fractions under adiabatic expansion with $T_{9i}=5$ and $\rho_i = 10^9 \text{ g cm}^{-3}$. The solid lines display the evolution due to a conventional α network, the circles show the evolution by the QSE-reduced α network. The Silicon group mass fraction is the sum of the mass fractions of ^{28}Si , ^{32}S , ^{36}Ar , ^{40}Ca , and ^{44}Ti . The Iron group mass fraction is the sum of the mass fractions of ^{48}Cr , ^{52}Fe , ^{56}Ni , and ^{60}Zn

difference has grown to 10% as T_9 nears 4. Fortunately this difference is negligible, since nuclear energy release has virtually ceased, with $< .2\%$ of the total energy release remaining.

Though energetically unimportant, nuclear reactions continue, resulting in significant changes in the smaller abundances. As pointed out by WAC, and discussed by HT98 in the context of a large nuclear network, the continued cooling results in the gradual freezeout of the photodisintegrations responsible for QSE. Typically, a photodisintegration only represents a significant flux if its Q value is less than $30 k_B T \sim 2.6 T_9$ MeV. The α captures which link silicon to nickel typically have Q values of 7-8 MeV, thus QSE begins to fail as T_9 approaches 3. However this same decline in temperature also reduces the rate of charged particle capture reactions, greatly reducing the amount of nucleosynthesis which occurs after T_9 drops below ~ 3.5 . The group abundances of the silicon and iron peak groups (which account for 99.9% of the mass), as calculated by the QSE-reduced α network after 18 ms have elapsed ($T_9=3.3$), differ by less than 1% from those of the conventional α network at the same point in time. Comparison of Columns 4 and 5 of Table 3 reveals larger variations among individual abundances, most notably, significant under estimation by the QSE-reduced network of the ^{48}Cr and ^{52}Fe abundances, with a small, compensatory over estimate of the ^{56}Ni abundance. These variations, factors of 2 and 4 for ^{52}Fe and ^{48}Cr , respectively, and 3% for ^{56}Ni signal the breakdown of the iron peak QSE group. With the steep decline in temperature and density, the flux upward from ^{52}Fe in the conventional network is no longer sufficient to provide the reduction in abundance which QSE and the sharply declining abundance of free α -particles requires.

As the temperature and density continue to decline, so to does the free α -particle abundance. Column 6 of Table 3 details the abundances after 255 ms have elapsed, with T_9 having dropped to .01, and all abundances having frozen out. Comparison of columns 4 and 6 reveals that the decline of the free α -particle abundance by 10^{-8} is the largest abundance variation beyond 18 ms. Since the more abundant species have effectively frozen out by the time T_9 approaches 3.5, comparison of columns 5 and 6 reveal that the predictions of the QSE-reduced network, frozen near $T_9=3.5$, also provide good abundance estimates, in addition to the excellent estimates of the rate of energy generation discussed earlier, in spite of the freezeout.

Figure 4 shows the evolution of another example of this explosive silicon burning model with $T_{9i} = 6$ and $\rho_i = 10^7 \text{ g cm}^{-3}$. The lower density in this case results in a slower expansion, with T_9 reaching 5, 4, and 3 after 77, 172, and 293 milliseconds, respectively. The nuclear evolution is similar to that portrayed in Figure 2 for the first 10 milliseconds, after which the declining temperature favors the iron peak group at the expense of lighter nuclei. Though the rate of cooling is relatively slow, the temperature drops too quickly for

Table 3: Comparison of network abundances for $T_{9i}=5.0$ and $\rho_i= 10^9 \text{ g cm}^{-3}$

Time (ms)	8.77		17.7		255
T_9	4.07		3.29		0.01
Nucleus	Y_{net}	Y_{qse}	Y_{net}	Y_{qse}	Y_{net}
^4He	7.90×10^{-7}	7.82×10^{-7}	1.04×10^{-8}	1.01×10^{-8}	1.94×10^{-14}
^{12}C	1.96×10^{-7}	1.96×10^{-7}	3.99×10^{-8}	3.23×10^{-8}	3.90×10^{-8}
^{16}O	7.34×10^{-7}	7.39×10^{-7}	5.26×10^{-7}	5.07×10^{-7}	5.27×10^{-7}
^{20}Ne	2.63×10^{-9}	2.63×10^{-9}	1.69×10^{-10}	1.48×10^{-10}	9.88×10^{-11}
^{24}Mg	2.24×10^{-6}	2.26×10^{-6}	2.88×10^{-7}	2.98×10^{-7}	2.80×10^{-7}
^{28}Si	7.65×10^{-3}	7.76×10^{-3}	7.58×10^{-3}	7.86×10^{-3}	7.58×10^{-3}
^{32}S	4.93×10^{-3}	4.96×10^{-3}	5.16×10^{-3}	5.15×10^{-3}	5.16×10^{-3}
^{36}Ar	1.43×10^{-3}	1.42×10^{-3}	1.27×10^{-3}	1.21×10^{-3}	1.27×10^{-3}
^{40}Ca	1.32×10^{-3}	1.30×10^{-3}	1.32×10^{-3}	1.22×10^{-3}	1.32×10^{-3}
^{44}Ti	7.07×10^{-6}	6.90×10^{-6}	1.96×10^{-6}	1.72×10^{-6}	1.69×10^{-6}
^{48}Cr	5.89×10^{-5}	5.58×10^{-5}	4.40×10^{-5}	1.19×10^{-5}	4.40×10^{-5}
^{52}Fe	7.17×10^{-4}	6.93×10^{-4}	6.33×10^{-4}	3.05×10^{-4}	6.33×10^{-4}
^{56}Ni	8.63×10^{-3}	8.60×10^{-3}	8.73×10^{-3}	9.04×10^{-3}	8.73×10^{-3}
^{60}Zn	6.18×10^{-8}	6.06×10^{-8}	3.26×10^{-9}	3.23×10^{-9}	4.38×10^{-10}

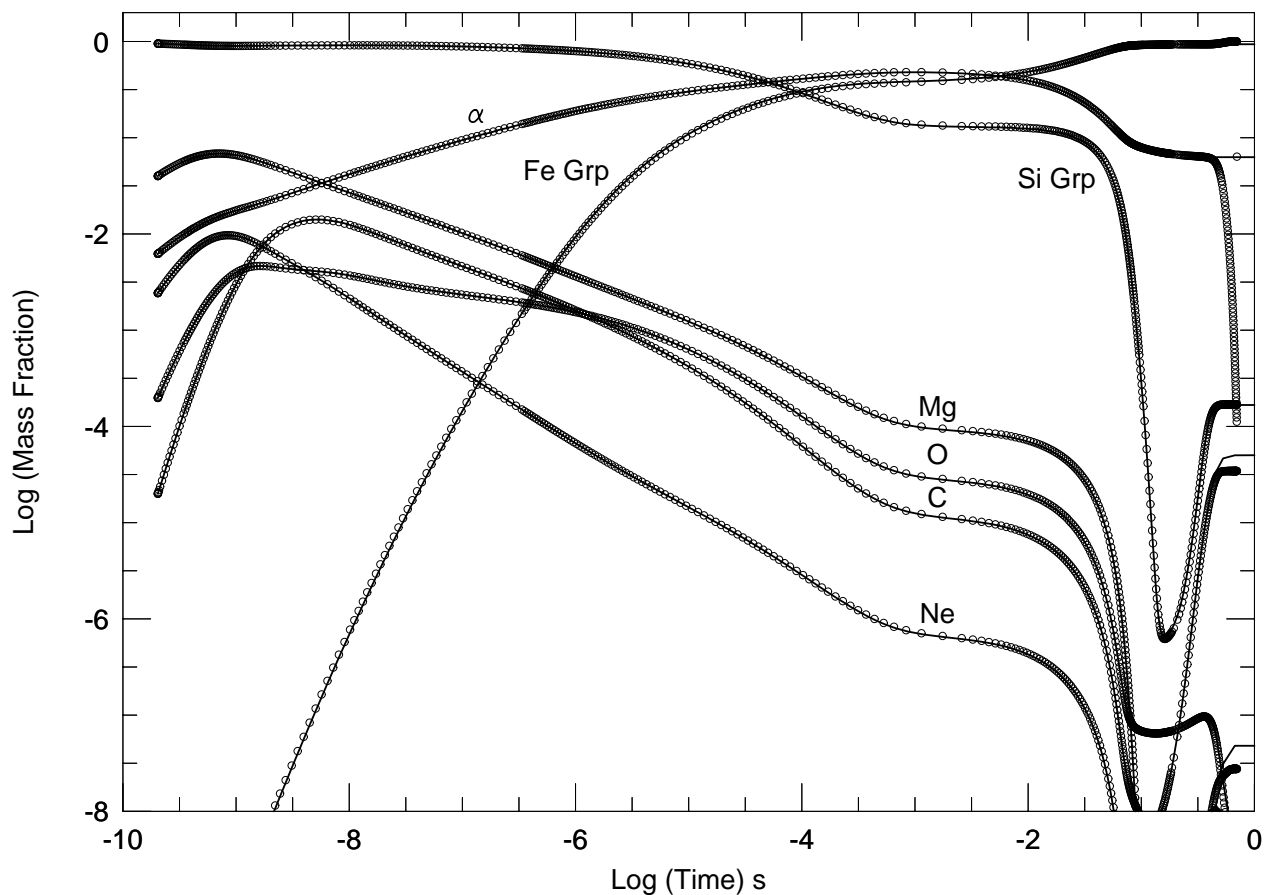


Fig. 4.— Evolution of the independent nuclear mass fractions under adiabatic expansion with $T_{9i}=6$ and $\rho_i = 10^7 \text{ g cm}^{-3}$. The solid lines display the evolution due to a conventional α network, the circles show the evolution by the QSE-reduced α network. The Silicon group mass fraction is the sum of the mass fractions of ^{28}Si , ^{32}S , ^{36}Ar , ^{40}Ca , and ^{44}Ti . The Iron group mass fraction is the sum of the mass fractions of ^{48}Cr , ^{52}Fe , ^{56}Ni , and ^{60}Zn

the large α -particle abundance to be completely incorporated into heavier nuclei, resulting in α -rich freezeout (see Arnett, Truran, & Woosley 1971, and Woosley, Arnett, & Clayton (1973). Even with this large overabundance of α -particles, the QSE-reduced network tracks the group abundances and rate of energy generation as reliably as it did under constant conditions until T_9 approaches 3.5. By the time 223 ms have elapsed ($T_9=3.5$), the largest relative difference, occurring in the small ($\sim 10^{-6}$) abundance of the silicon group, has grown to 9%. With only such small errors in abundance, it is not surprising that the difference in the rate of energy generation remains less than 1%. There is greater disparity between the individual abundances as calculated by the QSE-reduced network and those calculated by the conventional network.

As discussed by HT98 for a more complete nuclear network, in cases of α -rich freezeout the large α -particle abundance results in a relatively large nuclear flow upward into the silicon group. This flow gradually disrupts the QSE groups by increasing the abundance of the less massive members of the group while their QSE abundances drop sharply. Fortunately for our use of QSE to reduce the network, because of the large free α -particle abundance, these less massive members have only small abundances and thus the effects of this disruption are small. Comparison of abundances calculated by the conventional α network after 170 ms have elapsed ($T_9 \sim 4$) with those of its QSE-reduced counterpart (columns 2 and 3 of Table 4) shows the beginning of this process, with the abundances of ^{28}Si and ^{32}S much larger than QSE would predict. In spite of this breakdown in QSE, the abundances predicted for the more abundant members of the group and, as a result, the rate of energy generation, agree well. However as the temperature continues to drop, the disruption of the QSE groups by the large free α -particle abundance grows. By the time T_9 drops to 3 (columns 4 & 5 of Table 4), the under prediction by QSE of the smaller group abundances also effects the iron peak group. The abundances of the dominant nuclei, α , ^{56}Ni and ^{60}Zn , and hence the energy production, are still in good agreement, with the energy generation predictions differing by less than 1%.

Of particular importance, the abundance of ^{60}Zn is within 2% of that predicted by QSE. With a Q value of 2.7 MeV, $^{56}\text{Ni} + \alpha \leftrightarrow ^{60}\text{Zn} + \gamma$ remains balanced until significantly later than the reaction pairs connecting silicon to nickel. As the remaining photodisintegrations freeze out, the continued capture of the large abundance of α -particles results in a large number of α captures and significant abundances changes, the most prominent of which is the conversion of ^{56}Ni to ^{60}Zn . As late as an elapsed time of .35 seconds, with $T_9=2.6$ and $Y(^{60}\text{Zn}) = 1.5 \times 10^{-4}$, the abundance calculated for ^{60}Zn by the QSE-reduced network is within 5% of that predicted by the conventional network. As a result of this continued validity of QSE for the abundance of ^{60}Zn , the energy generation rate predicted by the QSE-reduced α network at an elapsed time of .35 seconds is only 11% greater than that

Table 4: Comparison of network abundances near freezeout for $T_{9i}=6.0$ and $\rho_i=10^7 \text{ g cm}^{-3}$

Time (s)	.174		.290		2.67
T_9	3.98		3.02		0.01
Nucleus	Y_{net}	Y_{qse}	Y_{net}	Y_{qse}	Y_{net}
^4He	1.73×10^{-2}	1.71×10^{-2}	1.62×10^{-2}	1.61×10^{-2}	1.57×10^{-2}
^{12}C	1.60×10^{-9}	1.58×10^{-9}	9.76×10^{-8}	9.62×10^{-8}	4.18×10^{-6}
^{16}O	4.24×10^{-9}	4.19×10^{-9}	5.51×10^{-9}	5.45×10^{-9}	2.16×10^{-10}
^{20}Ne	8.55×10^{-12}	8.46×10^{-12}	7.05×10^{-11}	6.96×10^{-11}	2.92×10^{-10}
^{24}Mg	4.38×10^{-12}	4.33×10^{-12}	3.25×10^{-11}	3.21×10^{-11}	2.00×10^{-9}
^{28}Si	1.92×10^{-11}	6.39×10^{-14}	1.92×10^{-10}	8.10×10^{-22}	2.95×10^{-9}
^{32}S	4.94×10^{-11}	4.42×10^{-12}	5.34×10^{-10}	2.14×10^{-17}	2.08×10^{-8}
^{36}Ar	2.60×10^{-10}	1.26×10^{-10}	2.46×10^{-9}	1.73×10^{-13}	1.59×10^{-7}
^{40}Ca	1.19×10^{-8}	1.12×10^{-8}	1.90×10^{-8}	6.44×10^{-9}	4.18×10^{-7}
^{44}Ti	4.73×10^{-9}	4.68×10^{-9}	1.71×10^{-7}	1.69×10^{-7}	3.26×10^{-6}
^{48}Cr	1.88×10^{-8}	1.51×10^{-8}	2.19×10^{-8}	1.26×10^{-14}	2.55×10^{-6}
^{52}Fe	1.59×10^{-5}	1.61×10^{-5}	9.26×10^{-7}	1.35×10^{-8}	4.50×10^{-6}
^{56}Ni	1.66×10^{-2}	1.66×10^{-2}	1.67×10^{-2}	1.67×10^{-2}	1.64×10^{-2}
^{60}Zn	6.50×10^{-6}	6.39×10^{-6}	4.23×10^{-5}	4.15×10^{-5}	2.97×10^{-4}

calculated by the full α network. As the temperature continues to drop, the continued α captures disrupt this last balanced reaction pair, converting even more ^{56}Ni into ^{60}Zn . Column 6 of Table 4 shows the abundances after 2.7 seconds have elapsed, by which time all of the abundances are frozen. While virtually all of the abundances have grown at the expense of those of free α -particles and ^{56}Ni , the most significant is a doubling of the abundance of ^{60}Zn after .35 seconds. Though the QSE-reduced network can not track the nuclear evolution to this point, the relatively small amount of energy released, less than 1% of that released over the first .35 seconds, makes this only a minor weakness.

4. The $\alpha 7$ network

While the preceding sections demonstrate the success of the QSE-reduced α network as a replacement for a conventional α network during silicon burning, it can not accurately calculate the evolution of $\vec{Y}^{\mathcal{F}}$ when QSE does not apply. Prior to silicon burning, the primary abundances of interest are those of α , ^{12}C , ^{16}O , ^{20}Ne , ^{24}Mg , and ^{28}Si . This subset of nuclei, which we will call \mathcal{R}' , is identical to \mathcal{R} , less ^{56}Ni . Thus evolution of a conventional α network for the 7 nuclei of the set \mathcal{R} can model these earlier burning stages nearly as well as the larger α network which evolves the entire set \mathcal{F} , with the only difficulty being small abundances of nuclei heavier than silicon. In combination with the QSE-reduced α network, one could hope to globally replace the full α network with a smaller network which evolves $\vec{Y}^{\mathcal{R}}$, using QSE where it applies. The principle uncertainty in the use of this combined network, which we have dubbed $\alpha 7$, is the the nature and timing of the transition to QSE.

The first necessary condition for QSE is that the temperature be in excess of 3×10^9 K, because, as discussed in §3, for lower temperatures the rates of photodisintegration are much smaller than the corresponding captures. An additional requirement for QSE to provide a good estimate of the abundances of heavier elements is that a significant fraction of the matter be composed of nuclei with $A > 24$. As long as the material is principally composed of lighter nuclei, like ^{12}C , ^{16}O , or ^{20}Ne , the production and destruction of free α -particles is dominated by reactions among these nuclei, rendering suspect QSE abundance predictions for the silicon and iron peak group nuclei based on these free α -particle abundances. Once these conditions are met, the abundances of the set \mathcal{R}' must be mapped in a suitable way into the initial abundances for the set \mathcal{G} which the QSE-reduced α network evolves.

One approach to this transition seeks to conserve the individual abundances of the sets \mathcal{R} and \mathcal{R}' across the transition, setting $\vec{Y}^{\mathcal{R}'} = \vec{Y}^{\mathcal{R}}$, and then calculating the initial values for $\vec{Y}^{\mathcal{G}}$ according to Eq. 7. Figure 5 displays the energy generation under constant conditions ($T_9=3$ and $\rho = 10^9 \text{ g cm}^{-3}$) for the $\alpha 7$ network using this *individual abundance*

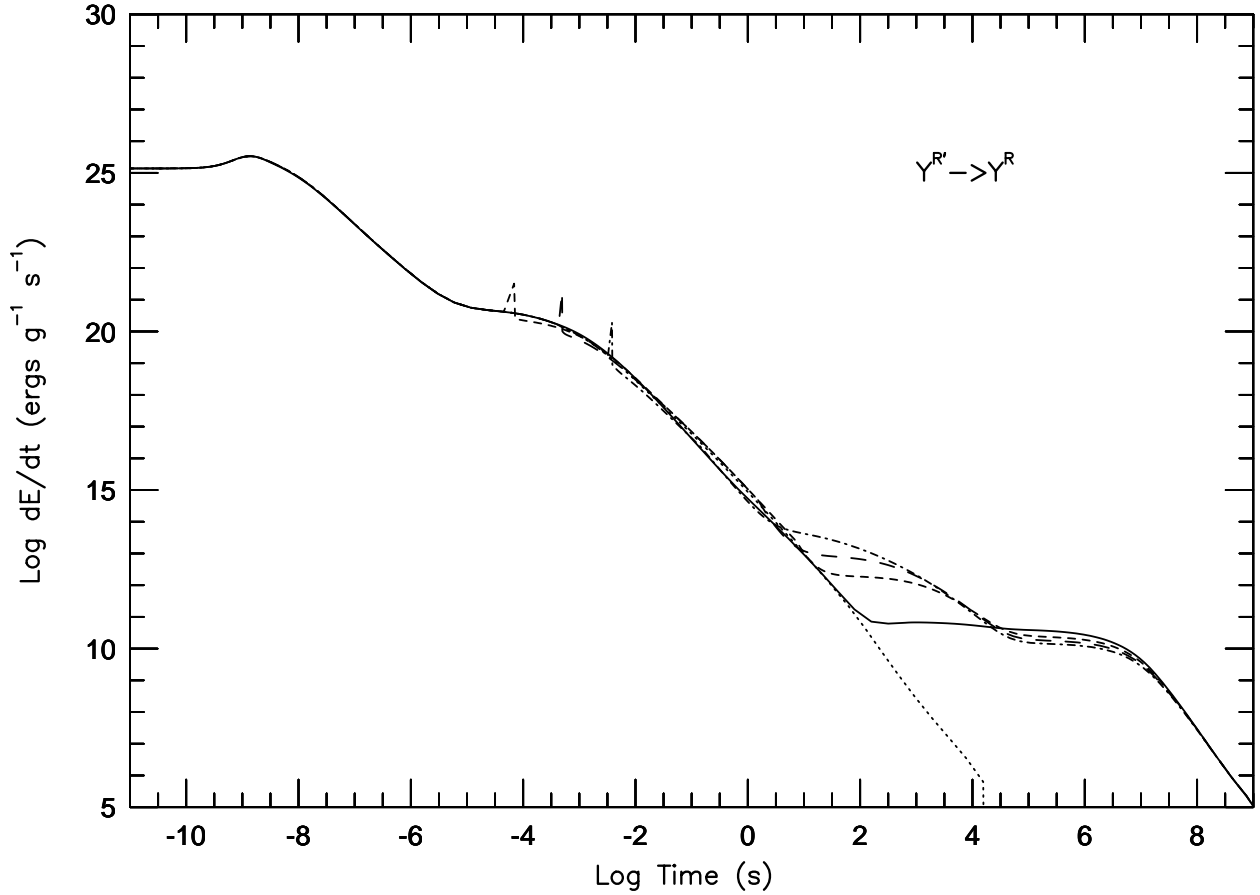


Fig. 5.— Comparison of the Energy generation by the full α network under constant thermodynamic conditions $T_9=3$ and $\rho = 10^9 \text{ g cm}^{-3}$ to the $\alpha 7$ network, assuming the individual abundance transition. The solid curve is the result of the conventional 14 element α network. The dotted curve shows the results of the $\alpha 7$ network, with the transition to QSE turned off. The short dashed, long dashed and dot dashed curves display the results of the $\alpha 7$ network, with the transition to QSE occurring when approximately 30%, 60% and 90% of the mass is in nuclei heavier than $A = 24$, respectively.

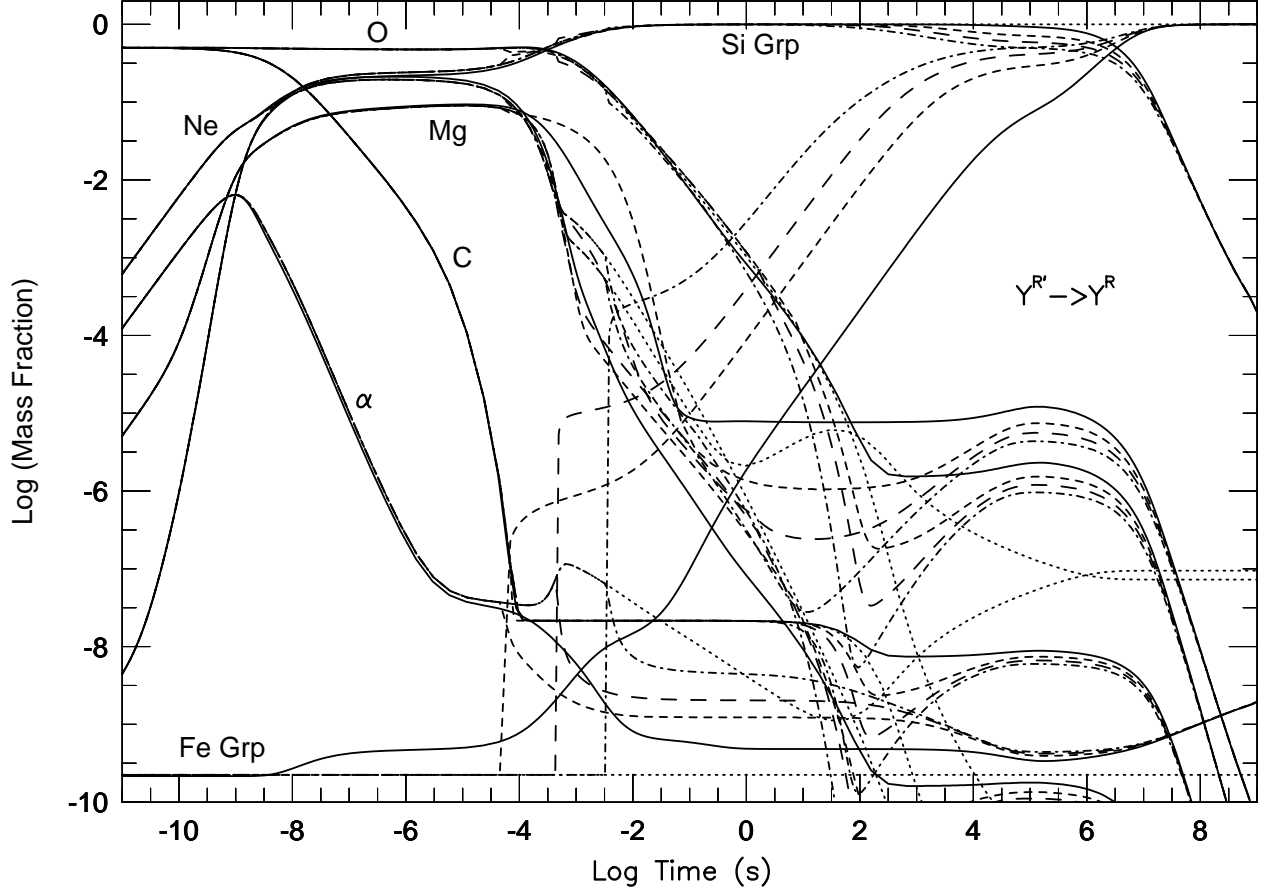


Fig. 6.— Comparison of the evolution of the independent mass fractions by the full α network under constant thermodynamic conditions $T_9=3$ and $\rho = 10^9 \text{ g cm}^{-3}$ to the $\alpha 7$ network, assuming the individual abundance transition. The solid curves are the result of the conventional 14 element α network. The dotted curves show the results of the $\alpha 7$ network with the transition to QSE turned off. The short dashed, long dashed and dot dashed curves display the results of the $\alpha 7$ network, with the transition to QSE occurring when approximately 30%, 60% and 90% of the mass is in nuclei heavier than $A = 24$, respectively.

(IA) approach to the transition. Figure 6 shows the group abundances for this same IA case. For Figures 5-8, the solid curves are the result of the conventional 14 element α network and the dotted curves show the results of the 7 element α network alone. The short dashed, long dashed and dot dashed curves display the results of the combined $\alpha 7$ network, with the transition to QSE occurring when approximately 30%, 60% and 90% of the mass is in nuclei heavier than $A = 24$, respectively. The spikes in the short dashed, long dashed and dot dashed curves seen in Fig. 5 result from errors in mass conservation at the transition. Treating $\vec{Y}^{\mathcal{R}'}$ as $\vec{Y}^{\mathcal{R}}$ results in an over estimate of the silicon and iron peak group mass fractions at the expense of ^{16}O , producing the spike in energy generation. This overabundance of iron also causes the excess energy production around 100 s and the corresponding dearth around 10^6 s.

If one examines the α -particle abundance (shown in Fig. 6) in the vicinity of 10^{-3} s, one sees that the 7 element α network, and its $\alpha 7$ network descendants, begin to overproduce free α -particles. In the conventional 14 element α network, these α -particles are capturing on ^{28}Si , populating the Si group at the expense of ^{28}Si , an option not allowed the smaller network. It is these overlarge abundances of ^{28}Si and free α -particles which cause the errors in mass conservation when QSE is first applied. A successful transition requires awareness that the abundance of ^{28}Si in the set \mathcal{R}' represents the total of all abundances above ^{24}Mg . In terms of $\vec{Y}^{\mathcal{G}}$, the capture of an α -particle on ^{28}Si does not change $Y_{\alpha G}$ or Y_{SiG} . If we consider $\vec{Y}^{\mathcal{G}}$ when nuclei heavier than ^{28}Si are not evolved, the sums in Eq. 7 disappear, leaving $Y_{\alpha G} = Y_{\alpha}$, $Y_{SiG} = Y(^{28}\text{Si})$, and $Y_{FeG} = Y(^{56}\text{Ni}) = \text{constant}$. Thus $\vec{Y}^{\mathcal{R}'}$ can also be mapped directly to $\vec{Y}^{\mathcal{G}}$. Since $\vec{Y}^{\mathcal{R}'}$ and $\vec{Y}^{\mathcal{G}}$ have the same normalization rule, mass is conserved. This approach seeks to conserve the abundances of the groups across the QSE transition, hence we refer to this as the *group abundance* (GA) transition. Figure 7 shows the energy generation, again for burning at a constant $T_9=3$ and $\rho = 10^9 \text{ g cm}^{-3}$, using this approach to transition. The results agree more closely with the conventional α network for all three values of the transition mass fraction, with the best results occurring for a transition mass fraction around 50%. The mass fractions predicted by this approach, shown in Figure 8, are also more reliable, though there are still significant discrepancies among the smaller mass fractions, particularly near the transition to QSE and for a transition mass fraction of 90%.

5. Conclusion

In this paper, we have demonstrated the ability of QSE to reduce the number of independent nuclear abundances which need to be evolved to track α -chain nucleosynthesis

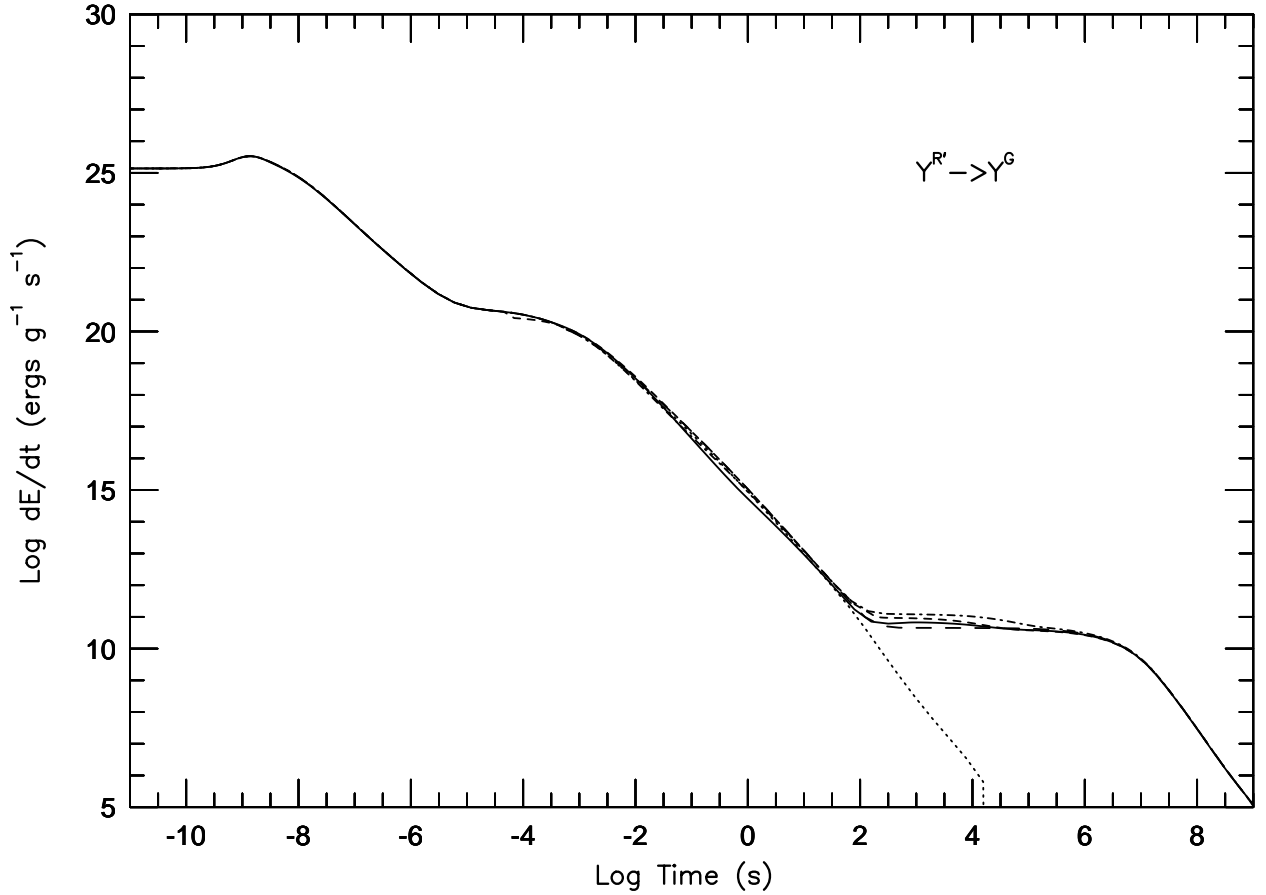


Fig. 7.— Comparison of the Energy generation by the full α network under constant thermodynamic conditions $T_9=3$ and $\rho = 10^9 \text{ g cm}^{-3}$ to the $\alpha 7$ network, assuming the group abundance transition. The solid curve is the result of the conventional 14 element α network. The dotted curve shows the results of the $\alpha 7$ network, with the transition to QSE turned off. The short dashed, long dashed and dot dashed curves display the results of the $\alpha 7$ network, with the transition to QSE occurring when approximately 30%, 60% and 90% of the mass is in nuclei heavier than $A = 24$, respectively.

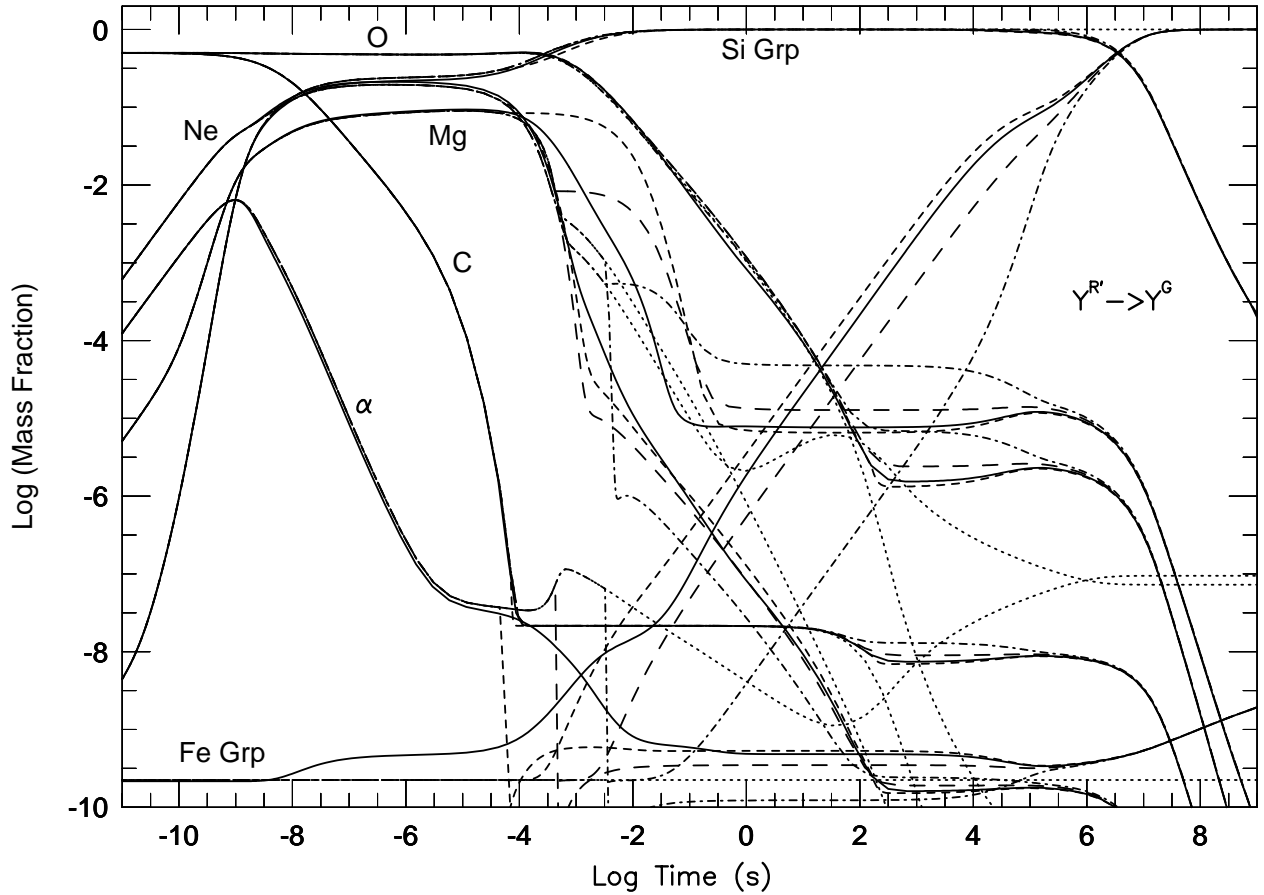


Fig. 8.— Comparison of the evolution of the independent mass fractions by the full α network under constant thermodynamic conditions $T_9=3$ and $\rho = 10^9 \text{ g cm}^{-3}$ to the $\alpha 7$ network, assuming the group abundance transition. The solid curves are the result of the conventional 14 element α network. The dotted curves show the results of the $\alpha 7$ network with the transition to QSE turned off. The short dashed, long dashed and dot dashed curves display the results of the $\alpha 7$ network, with the transition to QSE occurring when approximately 30%, 60% and 90% of the mass is in nuclei heavier than $A = 24$, respectively.

for silicon burning. An α network reduced in this fashion is capable of providing reasonable estimates of the nuclear energy generation and elemental production, even in cases where thermodynamic variations result in incomplete silicon burning or a freezeout rich in free α -particles. Computational, this reduction in the number of independent nuclear abundance variables offers two advantages. First, within the nuclear network calculation, the smaller number of variables results in a smaller matrix to build and solve. This speeds the nucleosynthesis calculation by a factor of 2 in the case of the α network, with the potential for much greater speed increases for larger networks. Second, the reduction in the number of nuclear variables also reduces the number of equations which must be solved within the encompassing hydrodynamic model, a matter of particular concern for models with large numbers of zones or grid points, especially multi-dimensional studies. The relative importance of these 2 advantages depends on the size of the network. As a rule of thumb, a PPM hydrodynamic code evolving 45 nuclear abundances spends roughly half its time on the network solution (Arnett 1998). Thus for small networks, like the α network, the reduction in necessary number of hydrodynamic equations is the paramount advantage.

In an effort to streamline the computation necessary for advanced nuclear burning stages, we have combined a smaller α network (for calculating the nuclear evolution from helium burning through oxygen burning) with this QSE based method. The resulting combined network, which we have dubbed $\alpha 7$, can be used in place of the full 14 element α network from helium burning through to NSE without significant errors in energy generation or nucleosynthesis. Such a combination offers the same reductions in the computational cost discussed above for silicon burning for all burning stages beyond H burning. In a future paper Hix, Freiburghaus, & Thielemann (1999), we will apply the method of QSE-reduction to larger nuclear networks, where the potential for improvement in speed and size is even greater.

The authors would like to thank P. Höflich, K. Nomoto, E. Oran and D. Arnett for fruitful discussions. This research was supported in part by NASA Grant NAG5-2888 and NSF Grant AST 9528110. FKT was supported in part by Swiss Nationalfonds grant 20-47252.96

REFERENCES

- Arnett, W.D. 1996, *Supernovae and Nucleosynthesis*, (Princeton Univ.:Princeton)
- Arnett, W.D. 1998, private communication

- Arnett, W.D., Truran, J.W., & Woosley, S.E. 1971, *ApJ*, 165, 87
- Bodansky, D., Clayton, D.D., & Fowler, W.A. 1968, *ApJS*, 16, 299
- Fowler, W.A., & Hoyle, F. 1964, *ApJS*, 9, 201
- Hix, W.R., Freiburghaus, C. & Thielemann F.-K. 1999, in preparation
- Hix, W.R., Thielemann F.-K. 1996, *ApJ*, 460, 869
- Hix, W.R., Thielemann F.-K. 1998, *ApJ*, submitted
- Press, W.H., Teukolsky, S.A., Vetterling, W.T. & Flannery, B.P. 1992, *Numerical Recipes* (Cambridge:Cambridge Univ.), second edition
- Thielemann, F.-K., Nomoto, K., Hashimoto, M. 1994, in *Supernovae, Les Houches, Session LIV*, eds. S. Bludman, R. Mochkovitch, J. Zinn-Justin, Elsevier, Amsterdam, p. 629
- Truran, J.W., Cameron, A.G.W., Gilbert, A. 1966, *Can. J. Phys.* , 44, 563
- Woosley, S.E. 1986, in *Nucleosynthesis and Chemical Evolution*, 16th Advanced Course of the Swiss Society of Astrophysics and Astronomy, ed. B. Hauck, A. Maeder, & G. Meynet (Geneva:Geneva Obs.), 1
- Woosley, S.E., Arnett, W.D., Clayton, D.D. 1973, *ApJS*, 26, 231